Aerospace Science and Technology 43 (2015) 471–477

Contents lists available at ScienceDirect

Aerospace Science and Technology

www.elsevier.com/locate/aescte

Experimental study of the effect of blade curvature and aspect ratio on the performance of a rotary-wing decelerator

Juan Francisco Martiarena *,[1], Vicente Nadal Mora [2], Joaquín Piechocki [3]

Universidad Nacional de La Plata, (1900) La Plata, Buenos Aires, Argentina

ARTICLE INFO

Article history:
Received 4 October 2013
Received in revised form 2 March 2015
Accepted 7 April 2015
Available online 14 April 2015

ABSTRACT

The effects of different blade configurations on a vertically falling rotating blade decelerator (pararotor) are studied. A pararotor model equipped with cambered plate blades with different curvatures was tested in a wind tunnel. The parameters measured were flow velocity, rotation velocity, the drag generated by the model, and the blade pitch angle. The parameters selected for the analysis of the results were the drag coefficient of the model and the velocity ratio (ratio between the falling and rotation velocities). These parameters were determined and compared with those obtained for flat-plate blades. Flat-plate blades with different aspect ratios were also tested and analyzed. The results obtained show that the velocity ratio increases with camber, and the equivalent drag coefficient remains unaltered by camber and aspect ratio variations.

1. Introduction

A rotary-wing decelerator, called a pararotor, is a device such as an unpowered helicopter rotor that spins in an autorotation regime. A drag force in the direction of the incident flow is generated over the rotor.

There are several kinds of application for these devices: for example, they can be used for atmosphere characterization in airport environments. The use of aerodynamic decelerators for these applications is focused on acquiring, through adequately mounted sensors, a complete map of pollutant emissions, wind shear detection, and microburst presence. The measurement of temperature, humidity, and pressure—factors that affect the low atmospheric boundary layer—could also be measured by an instrumented pararotor.

The principle of autorotation could be used for other applications, such as the recovery of reentry vehicles, guidance and control of projectiles or the guidance of aerodynamic devices. This principle shows particular interest in the application for unmanned vehicles on non-earthly atmospheres, due to its robustness, simplicity and energetical economy in the operation. Pararotor decelerator systems were compared with other methods of entry probe atmospheric deceleration by different authors [1–4] and were determined to show significant potential for application to mission concepts requiring controlled descent, low-velocity landing, and atmospheric research capability on planet exploration. They also show important applications in the military industry, due to its low weight, flexibility and easier integration.

An autorotation regime also appears in nature, in the reproduction strategy of certain plants. The samara seed spins as it falls, thus reducing its falling velocity and thereby increasing its dispersal distance. Several studies have examined samara aerodynamics. Crimi [5] developed a numerical study for computing the steady-state descent characteristics of the samara. Its device had a constant rate of descent and a periodical turning movement.

Rosen and Seter [6] present a theoretical model for samara aerodynamics based on blade element and momentum theories. They present a comparison between the experimental results obtained with a real samara and with an artificial samara. In another work, Seter and Rosen [7] present a numerical model for studying vertical autorotation stability, applying the small perturbations method to the dynamic equations for the samara. The influence of several parameters on the stability of the model is studied, and the results are compared by means of experimental tests.

In the field of pararotors, several works have been published. Nadal Mora, Sanz-Andrés, and Cuerva [8] developed a semi-empirical model to study the behavior of a low aspect ratio pararotor based on momentum theory. This model allows the ratio

* Corresponding author.
E-mail address: juanf.martiarena@gmail.com (J.F. Martiarena).
[1] Scholarship holder, Comisión de Investigaciones Científicas Provincia de Buenos Aires (CIC); Grupo de Ingeniería Aplicada a la Industria (UID GTA-GIAI), Departamento de Aeronáutica, Facultad de Ingeniería, Calle 116 entre 47 y 48.
[2] Professor, Grupo de Ingeniería Aplicada a la Industria (UID GTA-GIAI), Departamento de Aeronáutica, Facultad de Ingeniería, Calle 116 entre 47 y 48. Senior Member AIAA.
[3] Assistant Professor, Grupo de Ingeniería Aplicada a la Industria (UID GTA-GIAI), Departamento de Aeronáutica, Facultad de Ingeniería, Calle 116 entre 47 y 48.

http://dx.doi.org/10.1016/j.ast.2015.04.002
1270-9638/

Nomenclature

AR	aspect ratio	U_k	velocity ratio uncertainty
c	blade chord, m	U_{CDM}	pararotor drag coefficient uncertainty
C_{DM}	pararotor drag coefficient	U_T	tangential velocity, m/s
C_D	blade drag coefficient	U_R	relative velocity, m/s
C_L	blade lift coefficient	v_{io}	induced velocity at hover, m/s
C_{Lmax}	maximum lift coefficient	V_v	falling velocity, m/s
k	velocity ratio	α	angle of attack, deg
R	reference radius, m	β	blade pitch angle, deg
Re	Reynolds number	φ	flow incidence angle, deg
S_D	disk area, m^2	υ	kinematic viscosity, m^2/s
S_p	area of the two blades, m^2	ρ	air density, kg/m^3
T	net force over the model, N	ω	angular velocity, rad/s

between the falling velocity and the rotation velocity of device k to be determined for both the dimensionless falling and tangential velocities (V_v and U_T respectively), the pararotor drag coefficient CDM (drag in the falling direction), the blade angle of attack α, and the angle of incidence of the flow φ. In [9], Nadal Mora, Piechocki, and Sanz-Andrés present an experimental study on a rotary-wing decelerator model performed in a vertical wind tunnel. The test results agree with the dynamic behavior predicted by the analytical model developed by Nadal Mora and Sanz-Andrés [10], and Piechocki, Nadal Mora and Sanz-Andrés [11].

Regarding the stability analysis of pararotors, different types of stability appear depending on the relationship between the principal moments of inertia and aerodynamic and configuration parameters. Stability regions and stability types are described and analyzed in [8–11].

The interest of using low aspect ratio wings for pararotors is based on the possibility to fold wings over the main body to satisfy the transportation requirements. Main body height is limited, not only for practical reasons but also for gyroscopic stability reasons, and therefore, the aspect ratio is limited too. Moreover, low aspect ratio wings show specific stability and performance behavior that may have positive practical implications.

As the blades used on the studied have low aspect ratios, it is worth taking into consideration the work done by Pelletier and Mueller [12], who studied the aspect ratio effect (from 0.5 to 3.0) and the curvature effect for thin, flat plates, and 4% cambered plate wings. They concluded that 4% camber wings offer better aerodynamic characteristics than flat-plate wings for a given Reynolds number and aspect ratio. They also found that, for a given Reynolds number and aspect ratio, cambered blades showed higher C_L and C_D for a given angle of attack, and higher C_{Lmax} than the flat-plate blades.

Torres and Mueller [13] analyzed several configurations of low aspect ratio blade planforms, concluding that the parameter that most influences the characterization of the shape is aspect ratio, followed by the planform and the Reynolds number.

In [8–10,14] the behavior of pararotors equipped with low aspect ratio flat-plate blades was studied. These results are used as a reference for this work. In the present paper, the behavior of pararotors in relation to plate camber modifications is studied and analyzed. It is observed that the characteristic parameters k and C_{DM} vary as a consequence of modifications made to the plates used.

The experiment was carried out in a wind tunnel by varying the blade pitch angle from 2° to 8° and the flow velocity range from 4 to 11 m/s. The Reynolds number, defined as $R_e = \frac{V_v \cdot c}{\upsilon}$, for the tests varied between 80.000 and 125.000, approximately.

The aim of this study is to contribute to the knowledge of the effect of different blade types (camber and aspect ratio) on pararotor performance, and then broaden the available data to handle a desired performance.

Table 1
Blades' geometrical characteristics.

Blade type number	Span, m	Chord, m	Area, m^2	Camber, %	AR
1	0.088	0.138	0.012	0	0.63
2	0.088	0.138	0.012	4	0.63
3	0.088	0.138	0.012	8	0.63
4	0.138	0.088	0.012	0	1.56

2. Experimental setup

2.1. Model description and experimental setup

The experimental tests were carried out in the wind tunnel of the Departamento de Aeronáutica, Facultad de Ingeniería, Universidad Nacional de La Plata, Argentina (Aeronautics Department, School of Engineering, at the Universidad Nacional de La Plata). It is a closed-circuit tunnel with a rectangular test chamber (1.40 m wide × 1.00 m high × 1.72 m long). Air is propelled through it by a 37.3 kW direct current motor equipped with adjustable-pitch blades. The velocity can be controlled by an electronic system, which allows it to be set from 0 to 18 m/s.

The tested model was constructed based on an 88 mm diameter and 88 mm height aluminum cylinder with two lids (pararotor body). Two aluminum blades were attached to this main body in such a way that the pitch could be varied. The blades pitch angle axis location was at half-chord. The experimental setup prevents pararotor from any change on orientation due to pitch moments. The blades were removable, so that several geometrical configurations could be used.

The model was mounted with its spin axis parallel to the direction of the airstream.

Four types of blade were used for the tests. The first blade type tested was a thin rectangular flat plate of $AR = 0.63$, similar to those used in [8,9], which were taken as a reference. Two pairs of aluminum cambered plates were then tested, with cambers equal to 4% and 8% of the chord, and the fourth type of blade were flat plates of $AR = 1.56$. The cambered blades were constructed by means of a circular matrix with the required camber. The accuracy in the camber measure was 0.2%.

Table 1 summarizes the blades' geometrical characteristics.

A bedplate was designed and constructed to house the pararotor, which allowed the necessary measuring instruments to be integrated in the simplest possible way. In order to do this, a steel support was placed over a linear bearing guide to allow the model to move freely along its longitudinal axis. A suitably positioned

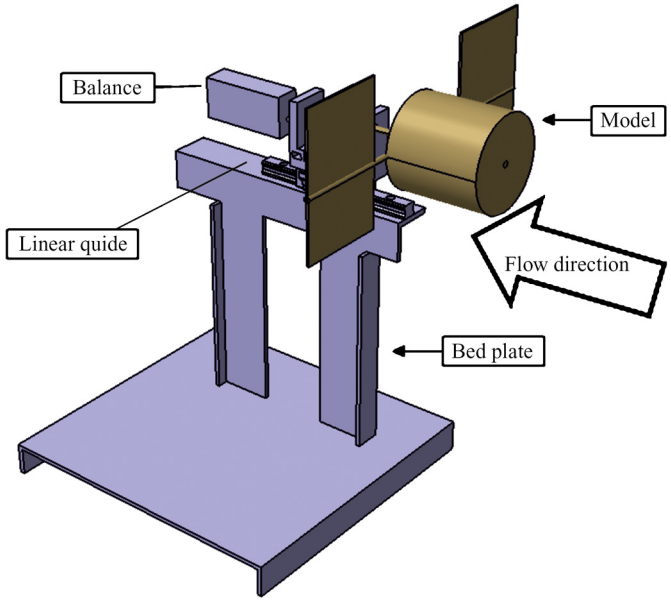

Fig. 1. Model, bedplate, and balance.

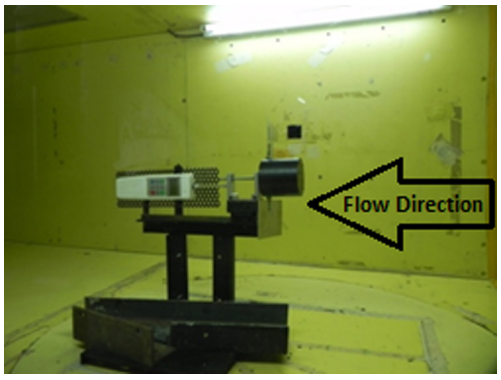

Fig. 2. Experimental set up inside the wind tunnel.

force sensor element allowed the traction of the model to be measured. Fig. 1 shows a schematic of the model and its bedplate.

Fig. 2 shows the experimental model set up inside the wind tunnel.

During the tests, the model traction, rotation velocity, stream wind velocity, and atmospheric parameters were measured for different blade pitch angles.

The experiments were repeated several times in similar conditions to verify reproducibility.

2.2. Measured parameters and instrumentation

The instrumentation used to measure the above mentioned parameters was as follows: the pararotor rotation velocity was measured by a laser tachometer (resolution 0.1 rpm (<1000 rpm), 1 rpm (>1000 rpm), range: 10 to 99,999 rpm); the air stream velocity, by a standard NPL Pitot-tube type and a micromanometer (resolution 0.5 Pa); the blade pitch angle, by a goniometer (resolution 0.1°); and the model drag force, by means of a digital balance (resolution 0.001 N, range: 0 to 10 N).

Ambient temperature was also measured (using a wet and dry bulb thermometer, resolution 0.1 °C), as was atmospheric pressure (with a digital pressure indicator, resolution 1 Pa, range: 74,500 to 115,000 Pa).

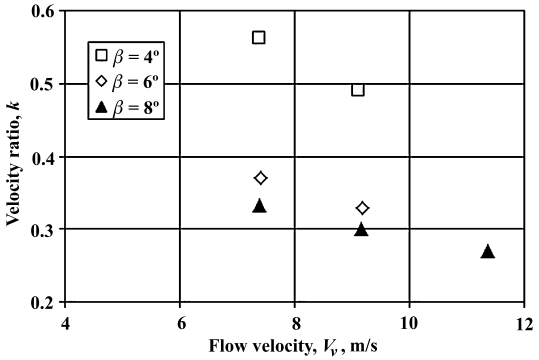

Fig. 3. Velocity ratio vs. flow velocity for blade type 1.

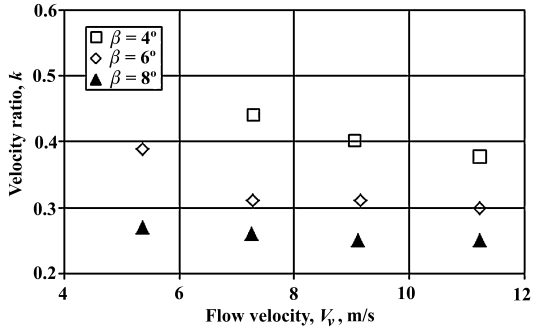

Fig. 4. Velocity ratio vs. flow velocity for blade type 2.

Two performance parameters were used to characterize pararotor performance. The pararotor drag coefficient is defined as:

$$C_{DM} = \frac{T}{\frac{1}{2}\rho V_v^2 S_p} \tag{1}$$

where T is the force exerted over the balance and S_p is the area of the two blades.

The velocity ratio, k, which is a dimensionless number defined as the ratio between the pararotor falling and blade tip velocities, can be expressed as follows:

$$k = \frac{V_v}{\omega R} \tag{2}$$

where ω is the spin velocity and the reference radius is $R = 0.138$ m.

3. Results

3.1. Test results

As mentioned above, the stream velocity, rotation velocity, and model drag were measured in order to determine the parameters k and C_{DM}. In the following figures, the average values of those parameters are presented as a function of the stream velocity for the blades tested for several blade pitch angles.

Figs. 3 to 6 show the velocity ratio versus the flow velocity for the blade types tested.

Figs. 7, 8 and 9 show the velocity ratio versus the blade step angle β for the tested blades.

Figs. 10 to 13 show the model drag coefficient versus the flow velocity for the blade types tested.

Table 2 summarizes the data obtained for the highest velocity tested ($V_v = 11$ m/s), which is taken as a reference velocity for comparison purposes.

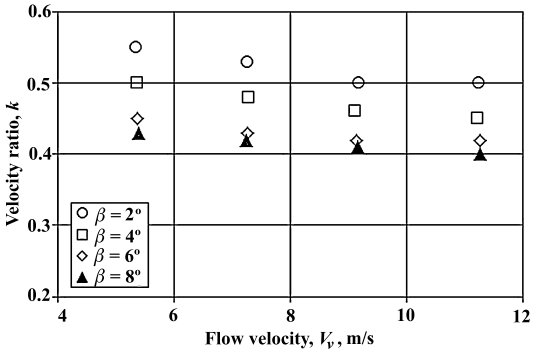

Fig. 5. Velocity ratio vs. flow velocity for blade type 3.

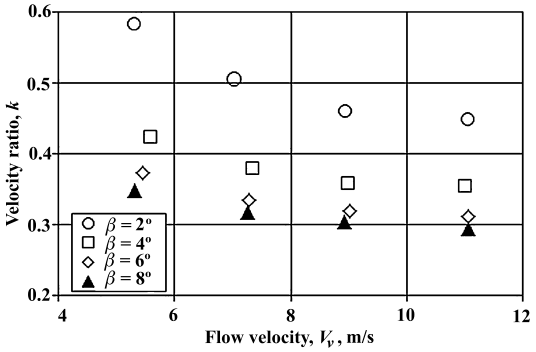

Fig. 6. Velocity ratio vs. flow velocity for blade type 4.

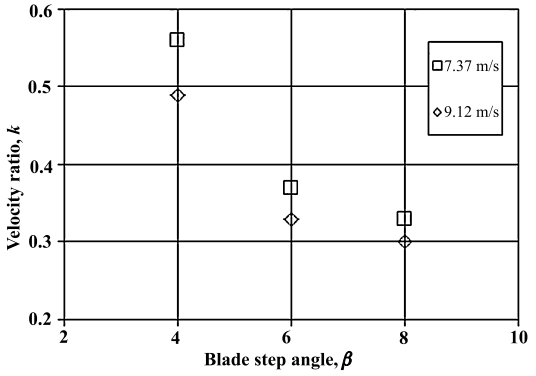

Fig. 7. Velocity ratio vs. blade step angle for blade 1.

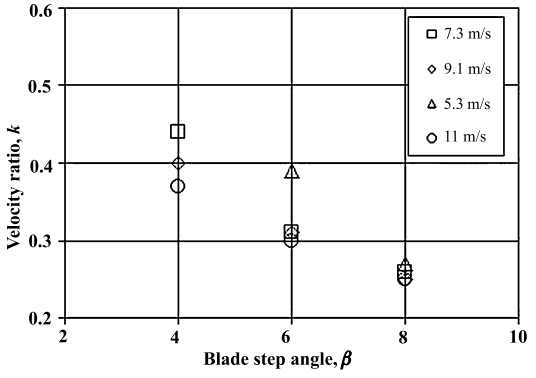

Fig. 8. Velocity ratio vs. blade step angle for blade 2.

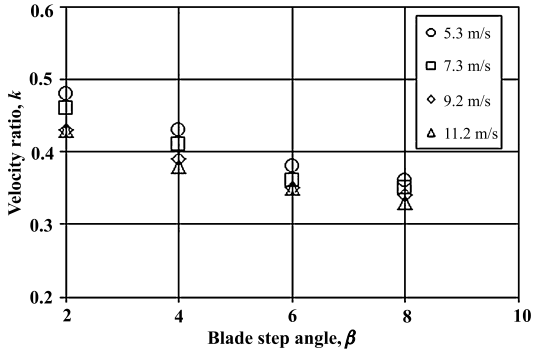

Fig. 9. Velocity ratio vs. blade step angle for blade 2.

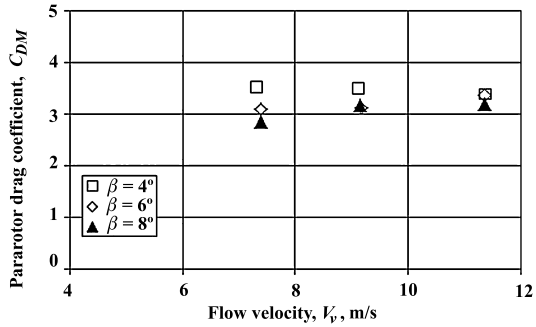

Fig. 10. Pararotor drag coefficient vs. flow velocity for blade type 1.

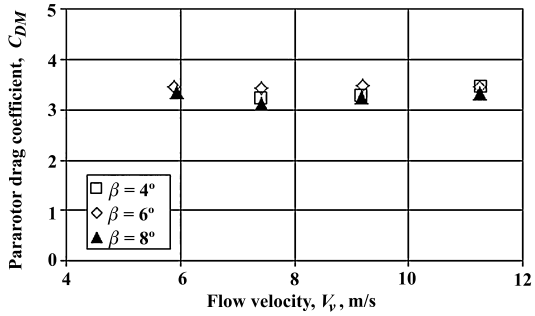

Fig. 11. Pararotor drag coefficient vs. flow velocity for blade type 2.

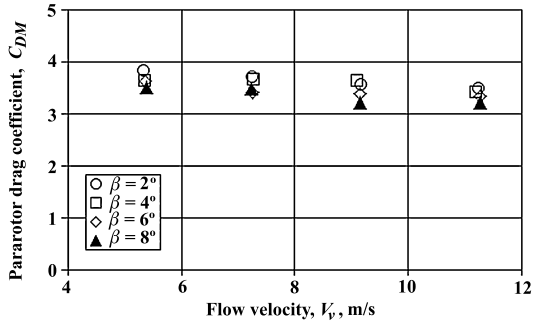

Fig. 12. Pararotor drag coefficient vs. flow velocity for blade type 3.

3.2. Determination of uncertainties

The uncertainties associated with the measurements were evaluated according to the methodology developed in [15]. From the analysis made, the relative combined uncertainty obtained for the velocity ratio k is in the order of 1%, and in the order of 5% for the pararotor drag coefficient C_{DM}.

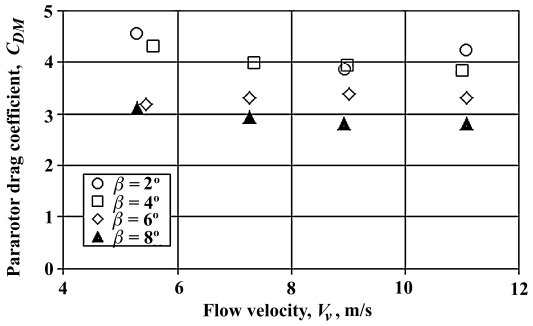

Fig. 13. Pararotor drag coefficient vs. flow velocity for blade type 4.

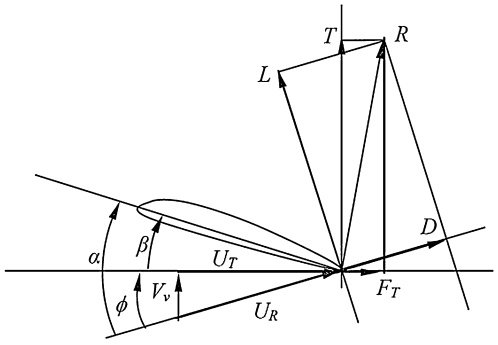

Fig. 14. Angles, net forces and velocity in the blade.

Table 2
Variations of k and C_{DM} for different blades vs. blade pitch angle, β.

Blade	$\beta = 2°$		$\beta = 4°$		$\beta = 6°$		$\beta = 8°$	
	k	C_{DM}	k	C_{DM}	k	C_{DM}	k	C_{DM}
1	0.42	3.43	0.375	3.35	0.31	3.35	0.28	3.1
2	–	–	0.38	3.4	0.31	3.4	0.26	3.1
3	0.5	3.38	0.45	3.36	0.42	3.3	0.4	3.22
4	0.45	4.22	0.35	3.83	0.31	3.32	0.29	2.82

Table 3
Test uncertainties (%).

Blade	$\beta = 2°$		$\beta = 4°$		$\beta = 6°$		$\beta = 8°$	
	U_k	U_{CDM}	U_k	U_{CDM}	U_k	U_{CDM}	U_k	U_{CDM}
1	–	–	–	–	0.56	3.22	0.51	3.24
2	–	–	0.65	3.06	0.53	3.20	0.44	2.59
3	0.73	4.5	0.66	4.60	0.61	4.98	0.59	4.84
4	0.79	3.27	0.63	3.53	0.55	4.12	0.52	4.82

The uncertainties associated with each measure are presented in percentage terms in Table 3.

4. Theoretical framework

The aerodynamics of low aspect ratio rotating wings is not well known. The flow pattern for these rotors differs widely from large aspect ratio wings rotors, where the blade element theory is valid. This theory assumes the existence of an almost two-dimensional flow in each plane perpendicular to the blade span. In the case of a low aspect ratio rotating wing, flow visualizations show a three-dimensional pattern with flow detached at the leading edge of the blades, as it would be the flow around a delta wing. The wing tip vortex reattaches the flow over the low aspect ratio wing, improving the performance parameters and increasing the operational blade angle of attack.

The mathematical model developed in [8] uses elements of the momentum theory to deduce the induced velocity due to the wake and by establishing the equilibrium of the forces that act over the blades required to attain the autorotation regime.

Regarding the velocity ratio, the theoretical approach based on the momentum theory developed in [8] is analyzed. Fig. 14 shows a blade element and the involved angles, forces and velocities in autorotation regime.

In Fig. 15 it can be seen that when the camber is augmented, the velocity ratio increases, due to the increment in C_D, as was observed in the experiments.

Figs. 16, 17 and 18 show a comparison between experimental tests and theoretical results. Following the analysis made in [8] we

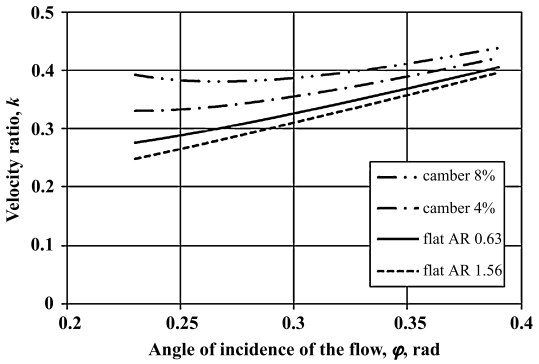

Fig. 15. Velocity ratio vs. angle of incidence of the flow.

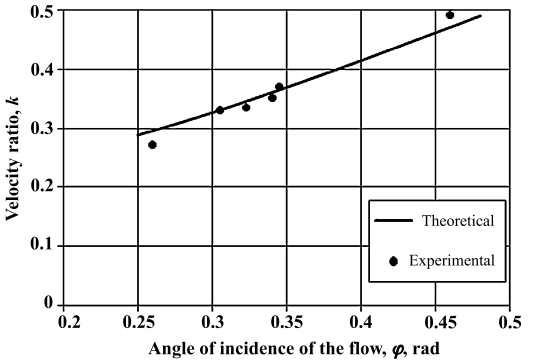

Fig. 16. Velocity ratio vs. angle of incidence of the flow for blade type 1.

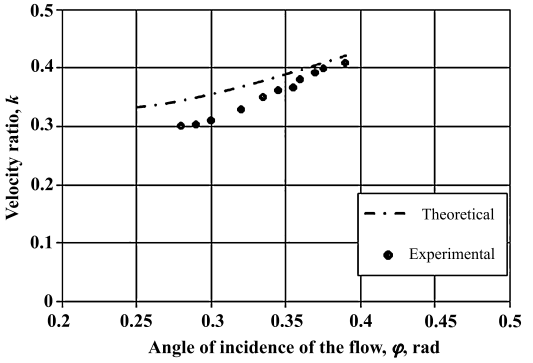

Fig. 17. Velocity ratio vs. angle of incidence of the flow for blade type 2.

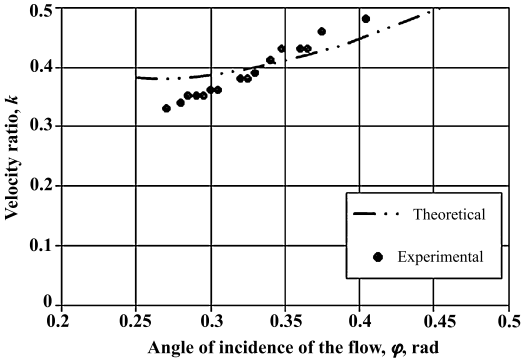

Fig. 18. Velocity ratio vs. angle of incidence of the flow for blade type 3.

can obtain an expression for k vs. φ.

$$k(\varphi) = \varphi + \frac{1}{\varphi^2}\frac{\sigma}{4}C_D \tag{3}$$

where φ is the flow incidence angle.

To explain the pararotor drag coefficient behavior, we can take the theoretical model developed in [8], based on the modelization of the net aerodynamic forces acting on the blades. The aerodynamic forces analysis can be seen in Fig. 11. We get that

$$L = \frac{1}{2}\rho U_R^2 S_p C_{L\alpha}\alpha \tag{4}$$

$$D = \frac{1}{2}\rho U_R^2 S_p C_D \tag{5}$$

The net force over the model is the sum of vectors L and D

$$T = L\cos(\varphi) + D\sin(\varphi) \tag{6}$$

It was defined in Eq. (1) the pararotor drag coefficient as the relation between the net force over the model, the dynamic pressure and the blades area.

If $\varphi << 1$ we can approach $T \cong L$. When the angular velocity decreases due to the drag increment, U_R does too, and L decreases. On the other side, the lift coefficient slope and the angle of attack increase due the camber. In the experiments it is seen that both effects are compensated and the net force over the model remains almost constant.

It is worth to mention that the effect of lateral skin friction of the cylinder and the friction of the bearings and linear guide, on which body is mounted for the tests, has also been assessed and, in consequence, neglected [8,16]. The drag force over the guide was measured to be in the order of 0.03 N, and so it was neglected.

The blade stiffness is such that the aerodynamic forces and torques produce a negligible elastic deformation, that was also assessed.

5. Conclusions

As previously mentioned, the pararotor blade camber and aspect ratio effects were analyzed for four models of blades.

The following conclusions can be drawn by analyzing the results presented in Table 2:

1- An increase in the velocity ratio is observed when the camber is increased. As expected from the theoretical analysis, the velocity ratio increases with the camber due to the effect of the drag coefficient increment. The behavior of the velocity ratio shows good agreement with the theoretical development, as is showed in Figs. 16, 17 and 18. Particularly for the blade type 1, the theoretical model describes with good quality the experimental behavior of the velocity ratio with the angle of incidence of the flow. For blade types 2 and 3, the theoretical model shows a mismatch of 15% regarding to the experimental results although it can be considered acceptable.
2- The model drag coefficient is not observed to vary significantly with camber, as deduced from the tests, for the highest velocity tested.
3- A reduction in the pararotor velocity ratio is shown when β is increased, for the same blade type and the same flow velocity. The increment in the blade pitch produces an increment in the angle of attack and consequently implies an increment of the lift generated by the blades. Hence, the horizontal component of the lift increases and the angular velocity too.
4- The velocity ratio does not vary significantly when the aspect ratio is increased.
5- The model drag coefficient increases at low blade pitch angles and decreases at high blade pitch angles when the aspect ratio is increased. It can be seen in Fig. 13 a gap between C_{DM} values for $\beta = 2, 4°$ and $\beta = 6, 8°$, that it is not observed for lower aspect ratio blades. This could be due to a change in flow configuration that may occur when β increases from 4 to 6°.

A first practical conclusion is that blade camber can be used to lower pararotor spin velocity, while maintaining its falling velocity, for a given weight model, as can be seen from the first conclusion listed above.

The effect of varying the blade aspect ratio for the cases analyzed shows a small influence on pararotor performance, so we can rule this out as a velocity control strategy.

The use of several blade types allows us to imagine several control strategies based on the aerodynamic characteristics of the blades. It appears that camber changes produce overall changes in performance.

Regarding stability, a change in blade camber introduces changes in the pararotors dynamics, as can be seen from [11]. So, response time and flight perturbances resistance could be modified by means of blade camber.

Conflict of interest statement

We wish to confirm that there are no known conflicts of interest associated with the publication *Experimental study of the effect of blade curvature and aspect ratio on the performance of a rotary-wing decelerator* and there has been no significant financial support for this work that could have influenced its outcome.

We confirm that the manuscript has been read and approved by all named authors and that there are no other persons who satisfied the criteria for authorship but are not listed. We further confirm that the order of authors listed in the manuscript has been approved by all of us.

We confirm that we have given due consideration to the protection of intellectual property associated with this work and that there are no impediments to publication, including the timing of publication, with respect to intellectual property. In so doing we confirm that we have followed the regulations of our institutions concerning intellectual property.

We understand that the Corresponding Author is the sole contact for the Editorial process (including Editorial Manager and direct communications with the office). He is responsible for communicating with the other authors about progress, submissions of revisions and final approval of proofs. We confirm that we have provided a current, correct email address which is accessible by the Corresponding Author and which has been configured to accept email from juanf.martiarena@gmail.com.

References

[1] G.E. Dorrington, Concept options for the aerial survey on Titan, Adv. Space Res. 47 (2011) 1–19.

[2] A. Kellas, The guided samara: design and development of a controllable single-bladed autorotating vehicle, Master of Science Thesis, Department of Aeronautics and Astronautics, Massachusetts Institute of Technology, 2007.

[3] T.J. Steiner, L.A. Young, Rotary wing decelerator use on Titan, in: Internationally Planetary Probe Workshop 8, EEUU, Portsmouth, 2011.

[4] L.A. Young, G. Briggs, E. Aiken, G. Pisanich, Rotary-wing decelerators for probe descent through the atmosphere of Venus, Defense Technical Information Center, 2004.

[5] P. Crimi, Analysis of samara-wing decelerator steady-state characteristics, J. Aircr. 25 (1) (1988) 41–47.

[6] A. Rosen, D. Seter, Vertical autorotation of a single winged samara, Trans. Am. Soc. Mech. Eng. 58 (1991) 1064–1070.

[7] D. Seter, A. Rosen, Stability of the vertical autorotation of a single winged samara, Trans. Am. Soc. Mech. Eng. 59 (1992) 1000–1008.

[8] V. Nadal Mora, A. Sanz-Andrés, A. Cuerva, Model of the aerodynamic behavior of a pararotor, J. Aircr. 43 (6) (2006) 1893–1903, http://dx.doi.org/10.2514/1.21435.

[9] V. Nadal Mora, J. Piechocki, A. Sanz-Andrés, Experimental research on a vertically falling rotating wing decelerator model, in: 19th AIAA Aerodynamic Decelerator Systems Technology Conference and Seminar, Williamsburg, VA, May 21–24, 2007, http://dx.doi.org/10.2514/6.2007-2538.

[10] V. Nadal Mora, A. Sanz, Stability analysis of a free falling pararotor, J. Aircr. 43 (4) (2006) 980–986, http://dx.doi.org/10.2514/1.16746.

[11] Joaquín Piechocki, Vicente Nadal Mora, Ángel Sanz Andrés, Pararotor dynamics: center of mass displacement from the blade plane—analytical approach, J. Aircr. (2014), http://dx.doi.org/10.2514/1.C032378, accessed April 3, 2014.

[12] A. Pelletier, T.J. Mueller, Low Reynolds number aerodynamics of low-aspect-ratio, thin/flat/cambered-plate blades, J. Aircr. (2000) 825–832.

[13] G. Torres, T. Mueller, Low aspect ratio wings aerodynamics at low Reynolds numbers, AIAA J. 42 (5) (2004), http://dx.doi.org/10.2514/5.9781600866654.0115.0141.

[14] V. Nadal Mora, A. Sanz, A. Cuerva, Experimental investigation of an autorotating-wing aerodynamic decelerator system, in: 18th AIAA Aerodynamic Decelerator Systems Technology Conference and Seminar, Munich, Germany, May 23–26, 2005, AIAA-Paper 2005-1635, http://dx.doi.org/10.2514/6.2005-1635.

[15] BIPM, Evaluations of Measurement Data – Guide to the Expression of Uncertainty in Measurement, first edition, BIMP, Sèvres Cedex, France, 2008.

[16] V. Nadal Mora, Comportamiento Aerodinámico de Sondas Atmosféricas en Entornos Aeroportuarios, Doctoral Thesis, Annex I, Universidad Politécnica de Madrid, Madrid, Spain, 2005, pp. Annex 1.2, Annex 1.19.